 CMES, vol.103, no.5, pp.281-313, 2014

Vertical Vibrations of an Elastic Foundation with Arbitrary Embedment within a Transversely Isotropic, Layered Soil

J. Labaki[1], **E. Mesquita**[2] **and R. K. N. D. Rajapakse**[3]

Abstract: This paper introduces a numerical model to investigate the vibratory response of elastic and rigid circular plates embedded in viscoelastic, transversely isotropic, three-dimensional layered media. In the present numerical scheme, the boundary-value problem corresponding to the case of time-harmonic concentrated and distributed axisymmetric vertical ring loads within a layered half-space is formulated according to an exact stiffness method. Its solution results in the required influence functions for the modeling of the present problem. The case of an embedded flexible plate is formulated in terms of a variational method. The deflection profile of the plate is written in terms of generalized coordinates combined with a polynomial approximation. These generalized coordinates are determined by the solution of the Lagrange's equation of motion, which involves the strain and kinetic energy of the flexible plate and energy due to contact tractions, as well as the potential energy due to the applied load. A set of Lagrange multipliers is incorporated into the equation of motion so that the boundary conditions at the plate edge are satisfied. The solution of the constrained Lagrangian function results in the deflection profile of the plate. The deflection profile of the embedded plate is shown for different governing parameters such as frequency and type of excitation and layering configuration of the surrounding medium. The present numerical scheme contributes to the study of dynamic response of buried foundations and anchors in non-homogeneous soils.

Keywords: Soil-foundation interaction, Transverse Isotropy, Layered Media, Elastic Foundations.

[1] Dept of Comp Mech, School of Mech Engrg, University of Campinas, Brazil.
[2] Dept of Comp Mech, School of Mech Engrg, University of Campinas, Brazil.
[3] Faculty of Applied Sciences, Simon Fraser University, Burnaby, Canada.

1 Introduction

The vibratory response of circular elastic plates interacting with transversely isotropic media has important practical applications in earthquake engineering and seismology. The case of an elastic plate embedded within transversely isotropic layered media is of particular interest to the analysis and design of foundations and anchors buried in the soil.

The study of elastic wave propagation in anisotropic media is quite sophisticated. State-of-the-art reviews on the wave propagation in such media are provided by Crampin, Chesnokov and Hipkin (1984) and Payton (1983), and in the references therein. More recently, Barros (1997) presented solutions for the time-harmonic behavior of three-dimensional viscoelastic transversely isotropic full- and half-spaces under time-harmonic loads. A rectangular coordinate system has been used in both cases. The present study builds on the solution derived by Wang in his PhD thesis (Wang, 1992), which was also reported in a paper by Rajapakse and Wang (1993). These authors derived Green's functions for a three-dimensional elastodynamic transversely isotropic full-space and half-space. A cylindrical coordinate system was used. The equation of equilibrium for time-harmonic motions were solved by introducing three potential functions, which were expanded in Fourier series, as introduced by Muki (1960). Because of the cylindrical coordinate system that was adopted, Hankel transforms were used in the solution. Semi-analytical solutions for Green's functions were derived by considering buried circular ring loads acting on the radial (r), circumferential (θ) and vertical directions (z). A particularization of Wang's solution for the horizontal and rocking response of a bi-material, transversely isotropic interface has been recently presented by Labaki, Mesquita and Rajapakse (2013).

Considerable efforts have been invested in the derivation of methods to study layered media. Some of the most recent ones include the works by Akbarov (2013) and Akbarov, Hazar and Eros (2013). A remarkable modeling scheme for layered media is the exact stiffness method, which resembles a finite element analysis. A stiffness matrix of the layered medium is assembled from the stiffness matrices of the layers in the same fashion that the stiffness matrix of a structure is assembled from the elementary stiffness matrices of its components. This method has been used by Wass (1972), Wass (1980), Kausel and Peek (1982), Mesquita and Romanini (1992) and Romanini (1995) to model multilayered isotropic media. Only a few results have been presented regarding the dynamics of multilayered anisotropic media. The most important ones to the present study are by Seale and Kausel (1989), Wang (1992) and Marques de Barros (2001). The first paper presented an extension of the thin-layer method to study the elastodynamics of a multilayered transversely isotropic half-space due to point loads. Wang (1992) and

Marques de Barros (2001) used an exact stiffness method to derive solutions for two-dimensional transversely isotropic layered media under time-harmonic loads in cylindrical and rectangular coordinates, respectively. Labaki (2012) extended Wang's solution for the three-dimensional case.

Different models of the flexural behavior of elastic plates have been presented in the literature. The book by Selvadurai (1979a) contains a detailed review of the various methods which have been used to deal with such problem. According to Rajapakse (1988), the variational method presented by Selvadurai (1979b, 1979c and 1980) is the most suitable to solve the problem of interaction between an elastic plate and its surrounding medium. One drawback of the variational method is the difficulty of obtaining an explicit representation of the traction field acting across the surface of the plate in response to the displacement field that is established. The integral equation system corresponding to the mixed boundary value problem only has an explicit solution for the case of the plate resting on the surface of the half-space or buried infinitely deep inside it [Rajapakse, (1988)]. Rajapakse (1988) derived a solution for the case of the elastic plate embedded at a finite depth inside an isotropic half-space. In Rajapakse's formulation, the deflection profile of the plate is described by a power series together with a term corresponding to a concentrated load derived according to the classical plate theory. The coefficients of the power series are determined through the minimization of a constrained energy functional involving the strain energy of the plate and of the surrounding medium and the potential energy of the external loads. Later on, Rajapakse (1989) presented a formulation that took into account the kinetic energy of a plate with mass. An analogous constrained Lagrangian equation of motion was constructed based on Lagrange multipliers, so that the boundary conditions at the plate edge could be satisfied. The resulting system of equations from the constrained Lagrangian functional was presented in a convenient matrix form, resembling the classical finite element method, and it has some advantages over the direct explicit variational scheme. His formulation considered the case of the plate resting on the surface of a three-dimensional, homogeneous, transversely isotropic half-space.

The present paper describes a numerical scheme for the investigation of the inertial response of an elastic circular plate embedded within viscoelastic, transversely isotropic, three-dimensional layered media. One example of the problem of interest is illustrated in Fig. 1. The flexible circular plate is modeled according to the solution derived by Rajapakse (1989). The case of a rigid plate is obtained as a particular case of the flexible plate. A model of layered media is presented according to the exact stiffness method [Wang, (1992)]. The model considers that each layer is a transversely isotropic, three-dimensional, viscoelastic medium, the response of which is given by the Green's function derived by Wang (1992). Time-harmonic

vertical, distributed or concentrated axisymmetric loads are considered.

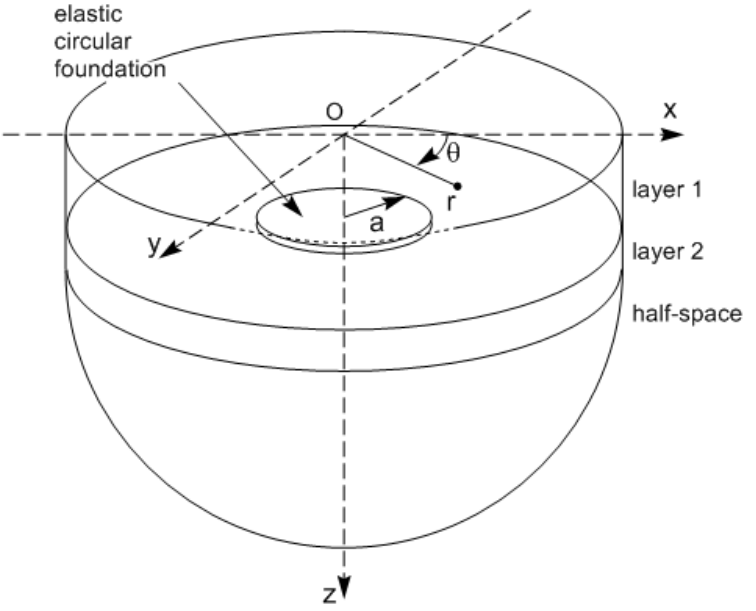

Figure 1: Elastic plate buried in a layered medium.

2 Governing equations

Consider a three-dimensional transversely isotropic full-space, the motion of which is described in cylindrical coordinates by the displacements $u_r(r, \theta, z)$, $u_\theta(r, \theta, z)$ and $u_z(r, \theta, z)$ in the r, θ and z directions, respectively. The cylindrical coordinate system O(r, θ, z) is positioned in such a way that its z-axis is orthogonal to the material's plane of isotropy. The displacements u_r, u_θ and u_z are related by the following coupled equations of motion [Wang, (1992)]:

$$\begin{aligned} & c_{11}\left(\frac{\partial^2}{\partial r^2}u_r+\frac{1}{r}\frac{\partial}{\partial r}u_r-\frac{u_r}{r^2}\right)+\frac{c_{11}-c_{12}}{2}\frac{1}{r^2}\frac{\partial^2}{\partial\theta^2}u_r+c_{44}\frac{\partial^2}{\partial z^2}u_r \\ & +\frac{c_{11}+c_{12}}{2}\left(\frac{1}{r}\frac{\partial^2}{\partial r\partial\theta}u_\theta+\frac{1}{r^2}\frac{\partial}{\partial\theta}u_\theta\right)-2c_{11}\frac{1}{r^2}\frac{\partial}{\partial\theta}u_\theta+(c_{13}+c_{44})\frac{\partial^2}{\partial r\partial z}u_z \\ & =\rho\frac{\partial^2}{\partial t^2}u_r \end{aligned} \tag{1}$$

$$\frac{c_{11}-c_{12}}{2}\left(\frac{\partial^2}{\partial r^2}u_\theta+\frac{1}{r}\frac{\partial}{\partial r}u_\theta-\frac{u_\theta}{r^2}\right)+c_{11}\frac{1}{r^2}\frac{\partial^2}{\partial\theta^2}u_\theta+c_{44}\frac{\partial^2}{\partial z^2}u_\theta$$
$$+\frac{c_{11}+c_{12}}{2}\left(\frac{1}{r}\frac{\partial^2}{\partial r\partial\theta}u_r-\frac{1}{r^2}\frac{\partial}{\partial\theta}u_r\right)+2c_{11}\frac{1}{r^2}\frac{\partial}{\partial\theta}u_r+(c_{13}+c_{44})\frac{1}{r}\frac{\partial^2}{\partial\theta\partial z}u_z \quad (2)$$
$$=\rho\frac{\partial^2}{\partial t^2}u_\theta$$

$$c_{44}\left(\frac{\partial^2}{\partial r^2}u_z+\frac{1}{r}\frac{\partial}{\partial r}u_z+\frac{1}{r^2}\frac{\partial^2}{\partial\theta^2}u_z\right)+c_{33}\frac{\partial^2}{\partial z^2}u_z$$
$$+(c_{13}+c_{44})\left(\frac{\partial^2}{\partial r\partial z}u_r+\frac{1}{r}\frac{\partial}{\partial z}u_z+\frac{1}{r}\frac{\partial^2}{\partial\theta\partial z}u_\theta\right)=\rho\frac{\partial^2}{\partial t^2}u_z \quad (3)$$

In Eqs. (1) to (3), ρ is the mass density of the medium and c_{ij} are elastic constants of the transversely isotropic material. Rajapakse and Wang (1993) derived a solution for this coupled equation system involving Hankel transforms. For the particular case of axisymmetry, in which there is no θ-dependency, the displacement fields and their corresponding stress fields are given by [Rajapakse and Wang, (1993)]:

$$u_i=\delta^2\int_0^\infty u_i^*\zeta d\zeta,\quad i=r,z \quad (4)$$

$$\sigma_{ij}=\delta^2\int_0^\infty \sigma_{ij}^*\zeta d\zeta,\quad i,j=r,z \quad (5)$$

In Eqs. (4) and (5), $\zeta=\lambda/\delta$, in which λ is the Hankel space variable. The kernels of displacement and stress involved in Eqs. (4) and (5) are given by:

$$u_r^*=a_1Ae^{-\delta\xi_1 z}+a_1Be^{+\delta\xi_1 z}+a_2Ce^{-\delta\xi_2 z}+a_2De^{+\delta\xi_2 z} \quad (6)$$

$$u_z^*=-\left(a_7Ae^{-\delta\xi_1 z}-a_7Be^{+\delta\xi_1 z}+a_8Ce^{-\delta\xi_2 z}-a_8De^{+\delta\xi_2 z}\right) \quad (7)$$

$$\sigma_{rr}^*=c_{44}\left(b_{11}Ae^{-\delta\xi_1 z}+b_{11}Be^{+\delta\xi_1 z}+b_{12}Ce^{-\delta\xi_2 z}+b_{12}De^{+\delta\xi_2 z}\right) \quad (8)$$

$$\sigma_{\theta\theta}^*=c_{44}\left(b_{61}Ae^{-\delta\xi_1 z}+b_{61}Be^{+\delta\xi_1 z}+b_{62}Ce^{-\delta\xi_2 z}+b_{62}De^{+\delta\xi_2 z}\right) \quad (9)$$

$$\sigma_{zz}^*=c_{44}\left(b_{21}Ae^{-\delta\xi_1 z}+b_{21}Be^{+\delta\xi_1 z}+b_{22}Ce^{-\delta\xi_2 z}+b_{22}De^{+\delta\xi_2 z}\right) \quad (10)$$

$$\sigma_{rz}^*=-c_{44}\left(b_{51}Ae^{-\delta\xi_1 z}-b_{51}Be^{+\delta\xi_1 z}+b_{52}Ce^{-\delta\xi_2 z}-b_{52}De^{+\delta\xi_2 z}\right) \quad (11)$$

in which, for i=1,2,

$$b_{1i}=b_{6i}=-\left[\delta^2\zeta^2\beta\vartheta_i-(\kappa-1)\delta^2\xi_i^2\right]J_0(\delta\zeta r) \quad (12)$$

$$b_{2i} = \left[\alpha\delta^2\xi_i^2 - (\kappa-1)\,\delta^2\zeta^2\vartheta_i\right] J_0(\delta\zeta r) \tag{13}$$

$$\frac{a_7}{\delta\xi_1} = \frac{a_8}{\delta\xi_2} = J_0(\delta\zeta r) \tag{14}$$

$$\frac{a_i}{\vartheta_i} = \frac{b_{5i}}{(1+\vartheta_i)\,\delta\xi_i} = -\delta\zeta J_1(\delta\zeta r) \tag{15}$$

In Eqs. (12) to (15), J_m represents the Bessel function of the first kind and m^{th} order. In the above equations the following parameterizations were also used:

$$\vartheta_{1,2} = \frac{\alpha\xi_{1,2}^2 - \zeta^2 + 1}{\kappa\zeta^2} \tag{16}$$

$$\xi_{1,2}(\zeta) = \frac{1}{\sqrt{2\alpha}}\left(\gamma\zeta^2 - 1 - \alpha \pm \sqrt{\Phi}\right)^{\frac{1}{2}} \tag{17}$$

$$\Phi(\zeta) = \left(\gamma\zeta^2 - 1 - \alpha\right)^2 - 4\alpha\left(\beta\zeta^4 - \beta\zeta^2 - \zeta^2 + 1\right) \tag{18}$$

$$\xi_3 = \pm\sqrt{\varsigma\zeta^2 - 1} \tag{19}$$

$$\begin{aligned} &\alpha = \frac{c_{33}}{c_{44}}, \quad \beta = \frac{c_{11}}{c_{44}}, \quad \kappa = \frac{c_{13}+c_{44}}{c_{44}}, \quad \varsigma = \frac{c_{11}-c_{12}}{2c_{44}}, \\ &\delta = \frac{\rho a^2}{c_{44}}\omega^2 \quad \text{and} \quad \gamma = 1 + \alpha\beta - \kappa^2 \end{aligned} \tag{20}$$

The coefficients A, B, C and D (Eqs. 6 to 11) are arbitrary functions that can be determined from the boundary and continuity conditions of a given problem. In the following section, these coefficients are determined for the case of a layered half-space under axisymmetric loads.

2.1 Exact stiffness method for layered media

Consider the three-dimensional multilayered medium shown in Fig. 2. Each of the N layers and the underlying half-space are made of a homogeneous transversely isotropic elastic material, the behavior of which is described by Eqs. (4) and (5). The material constants, mass density and thickness of the n^{th} layer are denoted by $c_{ij}^{(n)}$, $\rho^{(n)}$ and h_n, respectively.

Let $u_{i1}^{*(n)}$ denote the displacement in the i-direction (i=r,z) at the top surface of the n^{th} layer ($z=z_n$), and $u_{i2}^{*(n)}$ denote the displacement at the bottom surface of the n^{th} layer ($z=z_{n+1}$). The * superscript indicates Hankel transformed domain, such as the kernels from Eqs. (6) and (7). For example, in view of Eq. (6) this notation yields:

$$\begin{aligned} u_{r1}^{*(n)} =& a_1^{(n)}A^{(n)}e^{-\delta^{(n)}\xi_1^{(n)}z_n} + a_1^{(n)}B^{(n)}e^{\delta^{(n)}\xi_1^{(n)}z_n} \\ &+ a_2^{(n)}C^{(n)}e^{-\delta^{(n)}\xi_2^{(n)}z_n} + a_2^{(n)}D^{(n)}e^{\delta^{(n)}\xi_2^{(n)}z_n} \end{aligned} \tag{21}$$

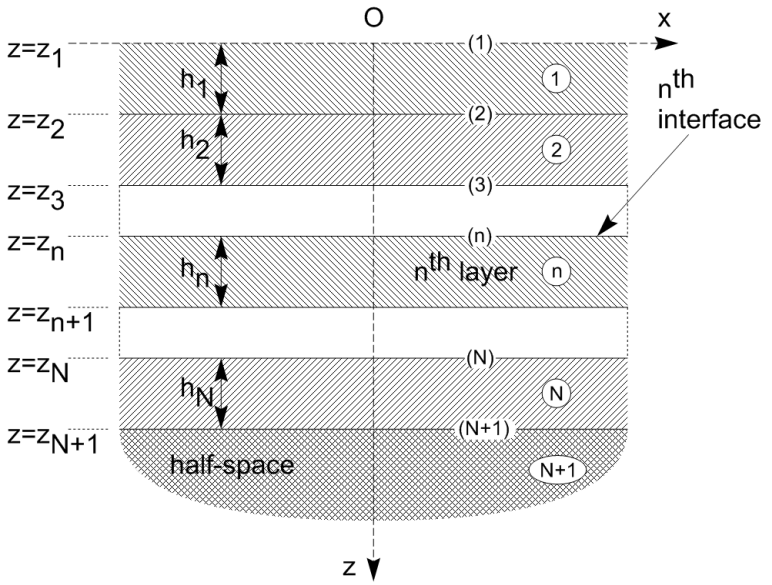

Figure 2: Geometry of a multilayered system.

$$\begin{aligned} u_{r2}^{*(n)} =& a_1^{(n)} A^{(n)} e^{-\delta^{(n)}\xi_1^{(n)} z_{n+1}} + a_1^{(n)} B^{(n)} e^{\delta^{(n)}\xi_1^{(n)} z_{n+1}} \\ &+ a_2^{(n)} C^{(n)} e^{-\delta^{(n)}\xi_2^{(n)} z_{n+1}} + a_2^{(n)} D^{(n)} e^{\delta^{(n)}\xi_2^{(n)} z_{n+1}} \end{aligned} \tag{22}$$

The two displacement components u_r and u_z from Eqs. (6) and (7) at the top and bottom surfaces of the n^{th} layer can be combined in one matrix equation:

$$u^{*(n)} = G^{(n)} a^{(n)} \tag{23}$$

where

$$u^{*(n)} = \left\langle \begin{array}{cccc} u_{r1}^{*(n)} & u_{z1}^{*(n)} & u_{r2}^{*(n)} & u_{z2}^{*(n)} \end{array} \right\rangle^T \tag{24}$$

$$a^{(n)} = \left\langle \begin{array}{cccc} A^{(n)} & B^{(n)} & C^{(n)} & D^{(n)} \end{array} \right\rangle^T \tag{25}$$

$$G^{(n)} = \begin{bmatrix} a_1 e_{1,n}^{-1} & a_1 e_{1,n}^{+1} & a_2 e_{2,n}^{-1} & a_2 e_{2,n}^{+1} \\ -a_7 e_{1,n}^{-1} & a_7 e_{1,n}^{+1} & -a_8 e_{2,n}^{-1} & -a_8 e_{2,n}^{+1} \\ a_1 e_{1,n+1}^{-1} & a_1 e_{1,n+1}^{+1} & a_2 e_{2,n+1}^{-1} & a_2 e_{2,n+1}^{+1} \\ -a_7 e_{1,n+1}^{-1} & a_7 e_{1,n+1}^{+1} & -a_8 e_{2,n+1}^{-1} & a_8 e_{2,n+1}^{+1} \end{bmatrix} \tag{26}$$

where

$$e_{i,j}^{\pm 1} = e^{\pm\delta^{(n)}\xi_i^{(n)} z_j}, \quad i = 1,2; \quad j = 1,2,\ldots,N+1 \tag{27}$$

The upper index (n) in the parameters a_i, i=1,2,7,8, is omitted in Eq. (26) for conciseness.

Similarly, let $\sigma_{ij1}^{*(n)}$ denote the ijth stress component (i,j=r,z) at the top surface of the nth layer (z=z$_n$), and $\sigma_{ij2}^{*(n)}$ denote the ijth stress component at the bottom surface of the nth layer (z=z$_{n+1}$). Let $p_{i1}^{*(n)}$ denote the traction acting at the top surface of the nth layer (n=1,N) in the i-direction (i=r,z), and $p_{i2}^{*(n)}$ denote the traction acting at the bottom surface of the nth layer in the i-direction. The corresponding matrix equation can be obtained from Eqs. (10) and (11) as:

$$p^{*(n)} = \sigma^{*(n)} = F^{(n)} a^{(n)} \tag{28}$$

where

$$\sigma^{*(n)} = \left\langle \begin{array}{cccc} -\sigma_{rz1}^{*(n)} & -\sigma_{zz1}^{*(n)} & \sigma_{rz2}^{*(n)} & \sigma_{zz2}^{*(n)} \end{array} \right\rangle^T \tag{29}$$

$$p^{*(n)} = \left\langle \begin{array}{cccc} p_{r1}^{*(n)} & p_{z1}^{*(n)} & p_{r2}^{*(n)} & p_{z2}^{*(n)} \end{array} \right\rangle^T \tag{30}$$

$$\frac{F^{(n)}}{c_{44}^{(n)}} = \left[\begin{array}{cccc} b_{51} e_{1,n}^{-1} & -b_{51} e_{1,n}^{+1} & b_{52} e_{2,n}^{-1} & -b_{52} e_{2,n}^{+1} \\ -b_{21} e_{1,n}^{-1} & -b_{21} e_{1,n}^{+1} & -b_{22} e_{2,n}^{-1} & -b_{22} e_{2,n}^{+1} \\ -b_{51} e_{1,n+1}^{-1} & b_{51} e_{1,n+1}^{+1} & -b_{52} e_{2,n+1}^{-1} & b_{52} e_{2,n+1}^{+1} \\ b_{21} e_{1,n+1}^{-1} & b_{21} e_{1,n+1}^{+1} & b_{22} e_{2,n+1}^{-1} & b_{22} e_{2,n+1}^{+1} \end{array} \right] \tag{31}$$

2.1.1 Underlying half-space

Consider the half-space shown in Fig. 2 ("layer" N+1). For the particular case of this semi-infinite medium, only the terms $A^{(N+1)}$ and $C^{(N+1)}$ are involved in the formulation, in order to satisfy Sommerfeld's radiation condition [Sommerfeld (1949); Zienkiewicz, Kelly and Bettess (1977)]. This results in a reduced form of Eqs. (23) and (28):

$$u^{*(N+1)} = G^{(N+1)} a^{(N+1)} \tag{32}$$

where

$$u^{*(N+1)} = \left\langle \begin{array}{cc} u_{r1}^{*(N+1)} & u_{z1}^{*(N+1)} \end{array} \right\rangle^T \tag{33}$$

$$a^{(N+1)} = \left\langle \begin{array}{cc} A^{(N+1)} & C^{(N+1)} \end{array} \right\rangle^T \tag{34}$$

$$G^{(N+1)} = \left[\begin{array}{cc} a_1 e_{1,N+1}^{-1} & a_2 e_{2,N+1}^{-1} \\ -a_7 e_{1,N+1}^{-1} & -a_8 e_{2,N+1}^{-1} \end{array} \right] \tag{35}$$

and

$$p^{*(N+1)} = F^{(N+1)} a^{(N+1)} \tag{36}$$

where

$$p^{*(N+1)} = \sigma^{*(N+1)} = \left\langle \begin{array}{cc} -\sigma_{rz1}^{*(N+1)} & -\sigma_{zz1}^{*(N+1)} \end{array} \right\rangle^T \tag{37}$$

$$\frac{F^{(N+1)}}{c_{44}^{(n)}} = \left[\begin{array}{cc} b_{51} e_{1,N+1}^{-1} & b_{52} e_{2,N+1}^{-1} \\ -b_{21} e_{1,N+1}^{-1} & -b_{22} e_{2,N+1}^{-1} \end{array} \right] \tag{38}$$

2.1.2 Stiffness matrix of the layers and half-space

Consider the vector $a^{(n)}$ shown in Eqs. (23) and (28), which contains the arbitrary functions $A^{(n)}$, $B^{(n)}$, $C^{(n)}$ and $D^{(n)}$. The vector $a^{(n)}$ is common to the expressions of displacements (Eq. 23) and stresses of each layer (Eq. 28). Equations (23) and (28) can be combined through $a^{(n)}$ into:

$$p^{*(n)} = F^{(n)} a^{(n)} = F^{(n)} \left(G^{(n)} \right)^{-1} u^{*(n)} = K^{(n)} u^{*(n)}; \quad n = 1,2,\ldots,N \tag{39}$$

In Eq. (39), the matrix $K^{(n)}$ is the stiffness matrix of layer n.

An analogous definition holds for the half-space. The vector $a^{(N+1)}$ shown in Eqs. (32) and (36) is common to the expressions of displacements (Eq. 32) and stresses of the half-space (Eq. 36). These equations can be combined through $a^{(N+1)}$ into:

$$\begin{aligned} p^{*(N+1)} &= F^{(N+1)} a^{(N+1)} \\ &= F^{(N+1)} \left(G^{(N+1)} \right)^{-1} u^{*(N+1)} = K^{(N+1)} u^{*(N+1)} \end{aligned} \tag{40}$$

In Eq. (40), the matrix $K^{(N+1)}$ is the stiffness matrix of the half-space ("layer" N+1).

Matrices $K^{(n)}$ depend on the material properties of the layer n (n=1,2,...,N,N+1) and its thickness, on the frequency of excitation and on the Hankel space variable ζ. The expression of $K^{(n)}$ is rather long and has to be determined numerically.

2.1.3 Stiffness matrix of the multilayered medium

Let $\wp_i^n$ denote the external concentrated or distributed axisymmetric load applied at the n^{th} interface of two layers, in the i-direction (i=r,z), such as described below in Section 2.2. This external load corresponds to the traction discontinuity at that interface, which in the Hankel transformed domain is given by:

$$H\{\wp_i^n\} = p_{i2}^{*(n-1)} + p_{i1}^{*(n)}; \quad i = r,z \tag{41}$$

Additionally, the kinematic continuity condition at the interface of any two layers is given mathematically by:

$$u_{i2}^{*(n-1)} = u_{i1}^{*(n)}; \quad i = r,z \tag{42}$$

Equation (41) is applied together with Eqs. (39) and (38) for all layers to form the following global stiffness matrix of the multilayered medium:

$$\wp^* = Ku^* \tag{43}$$

In Eq. (43), $\wp^*=\wp^*(\zeta)$ is the vector of external loads applied at the layer interfaces, given by Eq. (44); u*=u*(ζ) is the vector of resulting displacements of points of the interfaces, given by Eq. (45), and K=K(ζ) is the global stiffness matrix of the medium, given by Eq. (46). All these terms are in the transformed domain denoted by the upper index *, and depend on the normalized Hankel space parameter ζ.

$$\wp^* = \left\langle \begin{array}{cccccc} \wp_r^{*1} & \wp_z^{*1} & \dots & \wp_r^{*(N+1)} & \wp_z^{*(N+1)} \end{array} \right\rangle^T \tag{44}$$

$$u^* = \left\langle \begin{array}{cccccc} u_r^*(r,z_1) & u_z^*(r,z_1) & \dots & u_r^*(r,z_{N+1}) & u_z^*(r,z_{N+1}) \end{array} \right\rangle^T \tag{45}$$

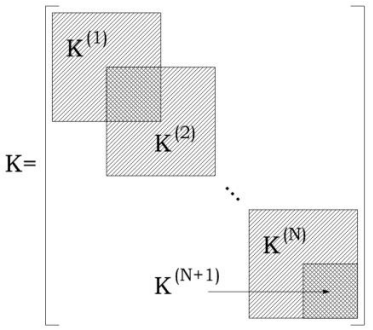

(46)

The solution of displacements from Eq. (43) must be integrated along ζ according to Eq. (4) to obtain the displacements at the layer interfaces in the physical domain. In this work, displacements in the i-direction due to loads in the j-direction are denoted by u_{ij} (i,j=r,z).

2.2 Description of loading

Let $\wp$ represent general axisymmetric loads in the physical domain, such as those that are applied at the layer interfaces (Eq. 44). One way of expressing these loads is by using Hankel transforms:

$$\wp = \mathrm{H}_m^{-1}\left\{\mathrm{H}_m\left\{\wp\right\}\right\} = \int_0^\infty \mathrm{H}_m\left\{\wp\right\} J_m\left(\zeta r\right) \zeta \, d\zeta \tag{47}$$

in which H_m and H_m^{-1} represent respectively the Hankel transform of order m and its inverse, and J_m represents Bessel functions of the first kind and order m [Abramowitz and Stegun, (1965)].

Consider an axisymmetric concentrated load of intensity p_0 applied as a ring of radius s, $\wp = p_0\delta(r-s)$. The representation of this load in the transformed domain is given by:

$$\mathrm{H}_0\left\{\wp\right\} = \int_0^\infty p_0 \delta\left(r-s\right) J_0\left(\zeta r\right) r \, dr = p_0 \cdot s \cdot J_0\left(\zeta s\right) \tag{48}$$

Based on this result, an expression for an analogous load distributed on an annular area with inner and outer radii s_1 and s_2 in the transformed domain can be derived:

$$\mathrm{H}_0\left\{\tilde{\wp}\right\} = \int_{s_1}^{s_2} p_0 s \cdot J_0\left(\zeta s\right) \, ds = \frac{1}{\zeta}\left[s_2 J_1\left(\zeta s_2\right) - s_1 J_1\left(\zeta s_1\right)\right] p_0 \tag{49}$$

The symbol $\wp$ with a tilde in Eq. (49) stands for distributed loads.

3 Vibrations of an embedded elastic plate

This section presents the formulation of a model of flexible circular plates. Kirchhoff theory of thin plates under small deflections is adopted. A trial function for the deflection profile of the plate is described by power series with a set of generalized coordinates. Lagrange's equation of motion of the plate is established, based on the assumed deflection profile. The minimization of the Lagrangian equation, under the constraint that it must satisfy the boundary conditions at the plate edge, results in the generalized coordinates that are used to describe the deflection profile of the plate.

3.1 Model of elastic plate

Consider an elastic, circular plate, with radius a (considered unit length parameter), thickness h, Young's modulus E_p, Poisson ratio ν_p and mass density ρ_p, embedded within an elastic media. The plate is under the effect of time-harmonic axisymmetric vertical loads.

The model of elastic plate adopted in this work comes from the classical plate theory. This model considers that the thickness h of the plate is small, compared with its radius a, and that the plate undergoes small deflections [Timoshenko and Woinowsky-Krieger, (1964)]. According to classical plate theory, all stress components can be expressed in terms of the deflection w(r) of the plate ($0 \leq r \leq a$). The linear partial differential equation that relates the deflection w(r) of the plate and the loading q(r) applied on it is [Timoshenko and Woinowsky-Krieger, (1964)]:

$$D\nabla^4 w(r) + \rho_p h \frac{\partial}{\partial t} w(r) = q(r); \quad 0 \leq r \leq a \tag{50}$$

in which

$$D = E_p h^3 / \left[12\left(1 - \nu_p^2\right)\right] \tag{51}$$

and

$$\nabla^4 = \frac{\partial^4}{\partial r^4} + \frac{2}{r}\frac{\partial^3}{\partial r^3} - \frac{1}{r^2}\frac{\partial^2}{\partial r^2} + \frac{1}{r^3}\frac{\partial}{\partial r} \tag{52}$$

In Eq. (50), q(r) is an arbitrary axisymmetric load applied perpendicularly to the surface of the plate. The term D in Eq. (51) is known as the bending (or flexural) rigidity of the plate. In the present case of axisymmetric bending, it involves only derivatives with respect to the variable r.

A trial solution for the deflection profile of the plate due to a uniformly distributed load of intensity $q(r)=q_0$ can be described by [Rajapakse, (1988)]:

$$w(r) = \sum_{n=0}^{N} \alpha_n w_n(r) = \sum_{n=0}^{N} \alpha_n r^{2n}; \quad 0 \leq r \leq 1 \tag{53}$$

The summation in Eq. (53) comprises an approximation for the deflection of the plate w(r) by power series. Each power profile r^{2n} is weighed by a generalized coordinate α_n (n=0,N).

Rajapakse (1988), Wan (2003), Selvadurai (1979c) and others investigated extensively the representation of an embedded plate with different sets of boundary conditions. According to Rajapakse (1988), the configuration of free edge is an accurate representation of the problem. This configuration, which states that the bending moment and shear force at the plate edge are zero, is used in the present work.

In view of the deflection profile established by Eq. (53), the expressions of bending moment Mr(r) and shear force Q(r) become [Timoshenko and Woinowsky-Krieger, (1964)]:

$$M_r(r) = -D \sum_{n=0}^{N} \alpha_n \left[2n(2n-1) + 2n\nu_p\right] r^{2n-2} \tag{54}$$

$$Q(r) = D\sum_{n=0}^{N} 4n^2(2n-2)\alpha_n r^{2n-3} \tag{55}$$

Substitution of the first boundary conditions of free edge, Mr(r=a=1)=0 in Eq. (54) yields:

$$\sum_{n=0}^{N} \alpha_n [2n(2n-1) + 2n\nu_p] = 0 \tag{56}$$

Substitution of the second boundary condition of free edge, Q(r=a=1)=0 in Eq. (55) yields:

$$\sum_{n=0}^{N} 4n^2(2n-2)\alpha_n = 0 \tag{57}$$

Equations (56) and (57) can be combined in a matrix equation involving a 2×(N+1) matrix [B] and a 2×1 vector {R} such that:

$$[B]\{\alpha\} = \{R\} \tag{58}$$

in which

$$B_{11} = B_{12} = B_{22} = 0 \tag{59}$$

$$B_{21} = 2(1+\nu_P) \tag{60}$$

$$B_{1j} = \left[4(j-1)^2 - 2(1-\nu_p)(j-1)\right]; \quad 3 \le j \le (N+1) \tag{61}$$

$$B_{2j} = 4(j-1)^2(2j-4); \quad 3 \le j \le (N+1) \tag{62}$$

$$R = \langle\ 0 \quad 0\ \rangle^T \tag{63}$$

$$\{\alpha\} = \langle\ \alpha_0 \quad \alpha_1 \quad \cdots \quad \alpha_N\ \rangle^T \tag{64}$$

3.2 Strain and kinetic energy of the flexible plate

The strain energy U_p of a thin elastic circular plate under flexural deformations is given by [Timoshenko and Woinowsky-Krieger, (1964); Rajapakse, (1988)]:

$$U_p = \int_0^1 \pi D\left[\left(\frac{d^2}{dr^2}w(r) + \frac{1}{r}\frac{d}{dr}w(r)\right)^2 - \frac{2(1-\nu_p)}{r}\frac{d^2}{dr^2}w(r)\frac{d}{dr}w(r)\right] r\,dr \tag{65}$$

In view of the deflection profile w(r) from Eq. (53), this strain energy can be expressed in a matrix form involving the generalized coordinates α:

$$U_p = \{\alpha\}^T [K^p] \{\alpha\} \tag{66}$$

In Eq. (66), [K^p] an (N+1)×(N+1) matrix, the terms of which are:

$$K_{1j}^p = K_{j1}^p = 0 \tag{67}$$

$$K_{ij}^p = \frac{4(i-1)(j-1)\pi D}{2i+2j-6}\left[4(i-1)(j-1)-2(1-\nu_p)(2i-3)\right];\ \ 2 \le i,j \le (N+1) \tag{68}$$

On the other hand, the kinetic energy of an elastic plate of mass density ρ_p and thickness h is given by [Timoshenko and Woinowsky-Krieger, (1964); Rajapakse, (1989)]:

$$T_p = \frac{h}{2}\int_0^1 \int_0^{2\pi} \rho_p (\dot{w}_p)^2 \, r\, dr\, d\theta \tag{69}$$

In view of Eq. (53), this kinetic energy can be written as:

$$T_p = \{\dot{\alpha}\}^T [M^p] \{\dot{\alpha}\} \tag{70}$$

in which

$$M_{ij}^p = h\rho_p \pi \left(\frac{1}{2(i+j-1)}\right); \quad 1 \le i,j \le (N+1) \tag{71}$$

3.3 Potential energy due to contact tractions

Let $t_z(r)$ represent the contact traction in the vertical direction. It is assumed that the influence of radial contact tractions is negligible [Rajapakse, (1988)]. The work done due to contact tractions is given by [Fung, (1965)]:

$$U_h = \tfrac{1}{2}\int_0^1 2\pi r \cdot t_z(r)\, w(r)\, dr \tag{72}$$

Let $t_{nz}(r)$ be the vertical contact traction field corresponding to each term $w_n(r)=r^{2n}$ of the power series in Eq. (53). Then,

$$t_z(r) = \sum_{n=0}^{N} \alpha_n t_{nz}(r) \tag{73}$$

A solution for $t_{nz}(r)$ by analytical methods is not feasible due to the complexity of the problem. A numerical solution is obtained by considering that the plate is made up of M concentric annular discs elements of inner and outer radii s_{1k} and s_{2k}

(k=1,M). The traction fields $t_{nz}(r_k)$ acting on each annular disc element are assumed to be uniformly distributed. For the discretized plate, it holds:

$$\sum_{k=1}^{M} u_{zz}(r_i, s_{1k}, s_{2k}, \omega)\, t_{nz}(r_k, \omega) = r_i^{2n}; \quad i = 1, M; \;\; n = 0, N \tag{74}$$

Equation (74) is solved for each n, resulting in $t_{nz}(r_k, \omega)$.

In Eq. (74), $u_{ZZ}(r_i, s_{1k}, s_{2k}, \omega)$ denotes the vertical displacement of a ring of radius r_i due to a vertical load that is uniformly distributed on an annular area of radii s_{1k} and s_{2k}. This influence function is obtained from the solution of Eq. (43).

In view of Eqs. (73) and (53), Eq. (74) can be written as:

$$U_h = \{\alpha\}^T \left[K^h\right] \{\alpha\} \tag{75}$$

In Eq. (75), $[K^h]$ is an (N+1)×(N+1) matrix, the terms of which are given by:

$$K_{ij}^h = \sum_{k=1}^{M} t_{(i-1)z}(r_k)\pi (s_{2k} - s_{1k}) \cdot r_k^{2j-1}; \quad 1 \le i, j \le (N+1) \tag{76}$$

3.4 Potential energy of the external loading

Let q_0 denote the intensity of a loading per unit area, that is uniformly distributed on a circular area of radius R≤a. A concentrated force can be represented by this loading by making R small. The potential energy E_q of this loading is given by [Zaman and Faruque, (1991)]:

$$E_q = 2\pi \int_0^R q_0 w(r)\, r\, dr \tag{77}$$

In view of the deflection profile w(r) from Eq. (53), the potential energy due to q_0 can be written in terms of generalized coordinates:

$$E_q = \langle F^q \rangle \{\alpha\} \tag{78}$$

in which $\langle F^q \rangle$ is a 1×(N+1) vector given by:

$$F_i^q = \pi q_0 \frac{R^{2i}}{i}; \quad 1 \le i \le (N+1) \tag{79}$$

3.5 Lagrangian formulation of the embedded plate

The Lagrangian function L of the system comprising the flexible plate, including contact tractions, can be expressed as [Washizu, (1982)]:

$$L = -U_p + T_p - U_h + E_p \tag{80}$$

Or, in terms of generalized coordinates:

$$L = -\{\alpha\}^T [K^p] \{\alpha\} + \{\dot{\alpha}\}^T [M^p] \{\dot{\alpha}\} - \{\alpha\}^T \left[K^h\right] \{\alpha\} + \langle F^q \rangle \{\alpha\} \tag{81}$$

In order to satisfy the boundary conditions at the plate edge, it is necessary to introduce a constraint Lagrange functional $\bar{L}_p$ that takes into account the boundary conditions expressed in Eq. (58):

$$\bar{L} = L + \{\lambda\}^T ([B] \{\alpha\} - \{R\}) \tag{82}$$

in which $\{\lambda\}$ is a 2×1 vector of Lagrange multipliers given by:

$$\{\lambda\} = \left\{ \begin{array}{cc} \lambda_1 & \lambda_2 \end{array} \right\} \tag{83}$$

The Lagrangian equation of motion for the plate can be written as:

$$\frac{d}{dt}\left(\frac{\partial}{\partial \dot{\alpha}_i}\bar{L}\right) - \frac{\partial}{\partial \alpha_i}\bar{L} = \{0\}, \quad 0 \le i \le N \tag{84}$$

And

$$\frac{\partial}{\partial \lambda_i}\bar{L} = \{0\}, \quad i = 1,2 \tag{85}$$

Substitution of Eq. (81) into (82) and subsequent differentiation according to Eqs. (84) and (85) results in:

$$\left[\begin{array}{cc} [K^s] & [B]^T \\ [B] & [0] \end{array} \right] \left\{ \begin{array}{c} \{\alpha\} \\ \{\lambda\} \end{array} \right\} = \left\{ \begin{array}{c} \{F\} \\ \{R\} \end{array} \right\} \tag{86}$$

where

$$[K^s] = -\omega^2 \left[M^p + (M^p)^T\right] + K^p + (K^p)^T + K^h + \left(K^h\right)^T \tag{87}$$

The numerical solution of Eq. (86) results in the generalized coordinates α_n (n=0,N). The deflection profile, bending moment and shear force on the plate can be obtained upon substitution of α_n (n=0,N) into Eqs. (53), (54) and (55), respectively.

4 Validation and numerical results

The hardest computational task that arises in the solution of the embedded plate is obtaining the solution of u_{ZZ} that appears in Eq. (74). In order to obtain this solution for each embedment configuration, Eq. (43) must be assembled and solved for each value of the space parameter ζ. The values of ζ for which Eq. (43) must be solved depend on the numerical scheme that is chosen to perform the integral expressed in Eq. (4). In the present implementation, a numerical solver of improper integrals, based on globally adaptive quadratures, is used for this purpose [Piessens, Doncker-Kapenga and Überhuber, (1983)]. Since the integrator is free to choose the values of ζ that are necessary to perform its integration scheme, it may select values that result in ill-conditioned matrices [K] (Eq. 43). In order to avoid this problem, a small damping η is introduced to all material constants according to Christensen's elastic-viscoelastic correspondence principle [Christensen (2010)]. A hysteretic damping model is adopted [Gaul (1999)].

4.1 Validation

The present implementation was used to reproduce the results from Rajapakse (1988). Rajapakse's problem corresponds to the case of an elastic massless plate at an arbitrary depth H within an isotropic half-space (Fig. 3a). Uniformly distributed static loads (ω=0) on the surface of the plate are considered. In the present implementation, the different depths of embedment H are obtained by considering a single layer on top of the plate and a half-space below it. The cases labeled H/a=0 correspond to the case of the plate resting on the surface of the half-space. The case of distributed loads are reproduced by making the outer radius of the loading area R/a=1. The case of concentrated loads is represented by making R/a=10^{-3}. A discretization of M=20 annular disc elements and N=6 generalized coordinates are used in all results. Numerical convergence studies performed within this work and in the work by Rajapakse (1988) showed that these parameters (M=20 and N=6) furnish accurate results for the investigated cases.

Figure 4 presents the normalized central displacement w*(r=0) and bending moment M_r^*(r) of the plate under the effect of distributed static loads (ω=0). These and other normalizations, such as the differential displacement w_d^* and the normalized shear force Q*(r), are defined as:

$$w^*(r) = \frac{w(r)\,E_s}{q_0\,(1-\nu_s^2)\,a} \quad \text{and} \quad w_d^* = \frac{E_s\,[w(0)-w(a)]}{q_0\,(1-\nu_s^2)\,a} \tag{88}$$

$$M_r^*(r) = \frac{M_r(r)}{q_0 \cdot a^3} \quad \text{and} \quad Q^*(r) = \frac{Q(r)}{q_0 \cdot a^2} \tag{89}$$

$$K_r = \left(1 - \nu_s^2\right) \frac{E_p}{E_s} \left(\frac{h}{a}\right)^3 \tag{90}$$

in which E_s and ν_s are the Young's modulus and Poisson ratio of the surrounding medium, q_0 is the intensity of the loading per unit area, and h is the thickness of the plate. For fixed values of E_s, ν_s, h and a, the relative rigidity K_r (Eq. 90) represents essentially the stiffness of the plate. As this normalized parameter tends to a large value, the plate tends to a rigid plate. The present implementation can be used to study the vibration of rigid plates by making K_r large.

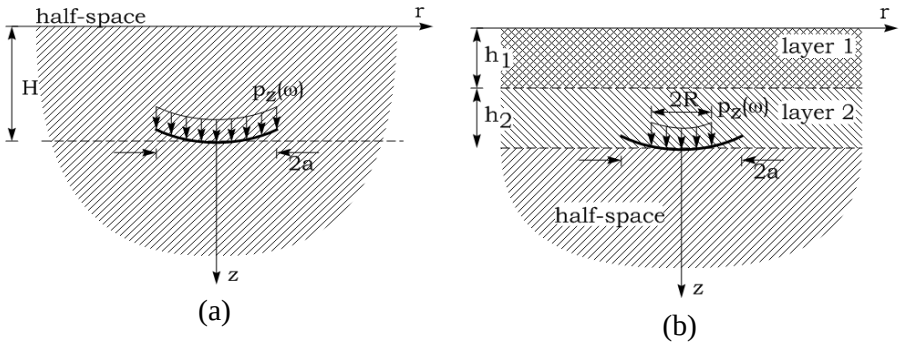

Figure 3: (a) embedment of the elastic plate at an arbitrary depth H within a homogeneous half-space, and (b) embedment at the interface of an arbitrary number of layers and a half-space.

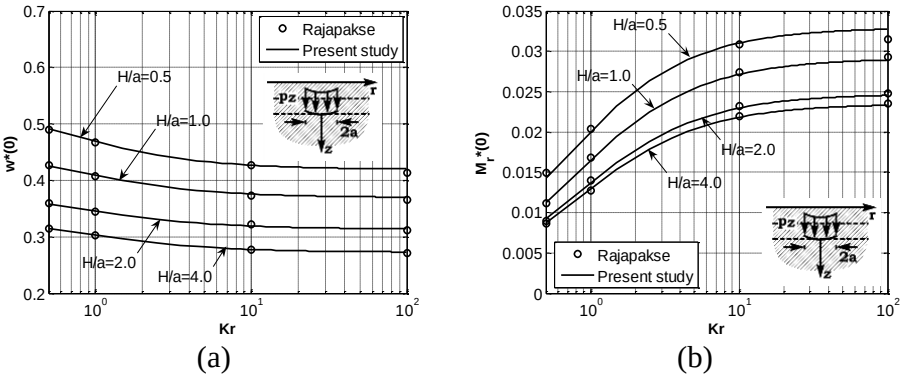

Figure 4: Response of an elastic plate at different embedments within an isotropic half-space, due to a uniformly distributed static load - a) displacement $w^*(r=0)$ and b) bending moment $M_r^*(r=0)$.

The present implementation has also shown good agreement with the results by Rajapakse (1988) for the case of concentrated loads.

Figure 5 shows the case of a rigid plate at the interface between an isotropic half-space and two layers of unit thickness. These results are presented in terms of the normalized dynamic vertical compliance defined by:

$$C_{ZZ}(a_0) = \frac{w(r=0,a_0)\cdot E_s}{\pi q_0 a} \tag{91}$$

in which a_0 is the normalized frequency of excitation defined by:

$$a_0 = \frac{\omega \cdot a}{c_S} \tag{92}$$

in which c_S (c_S^2=c_{44}/ρ) is the shear wave propagation speed in the homogeneous surrounding medium.

These results agree with the ones presented by Pak and Gobert (1992) for vertical vibration of a massless rigid circular plate embedded at a depth H/a=2 inside an isotropic half-space. The compliance shown in Fig. 5 is normalized by the vertical static compliance of a plate resting on the surface of the half-space, $C^0_{ZZ}(a_0=0)$, whose closed-form solution was derived by Pak and Gobert (1992).

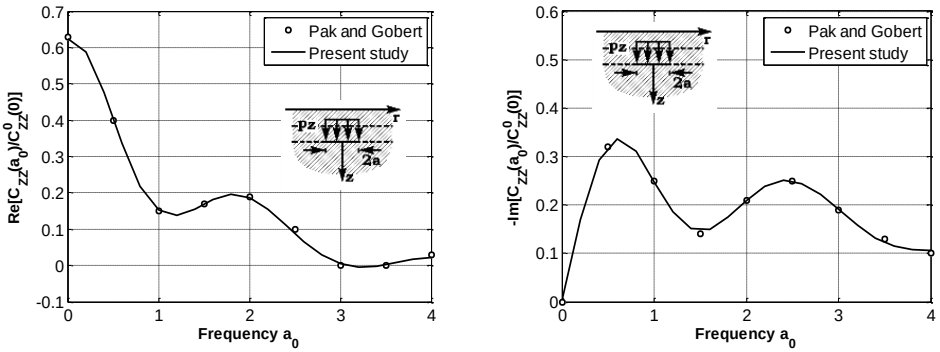

(a) (b)

Figure 5: Normalized vertical dynamic compliance of a rigid plate between two isotropic layers of unit thickness and an isotropic half-space.

4.2 Influence of the frequency of excitation

The present model of embedded plates is capable of dealing with the case of time-harmonic loads. Figures 6 and 7 show the influence of the frequency of excitation

on the central deflection (r/a=0) of a flexible massless plate (K_r=0.5). Uniformly distributed loads are considered. Different depths of embedment H for the plate are considered. The plate is situated between the half-space and the first layer above it. All layers and the half-space are homogeneous isotropic media.

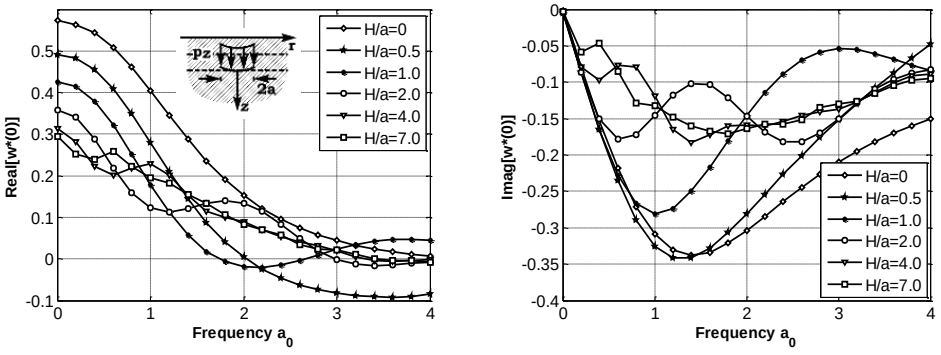

(a) (b)

Figure 6: Influence of the frequency of excitation on the central deflection of the flexible plate under uniformly distributed loads.

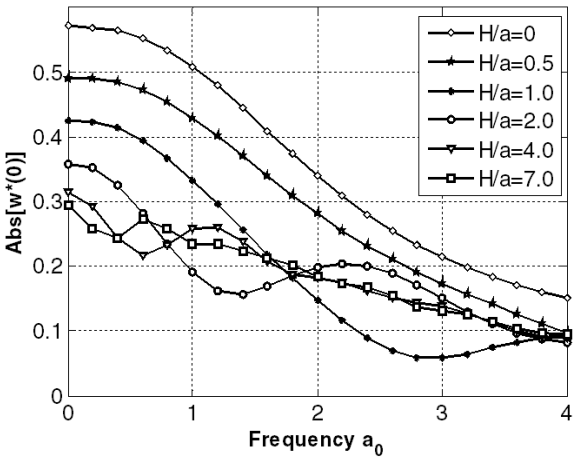

Figure 7: Influence of the frequency of excitation on the central deflection of the flexible plate under uniformly distributed loads – Absolute value of the middle point deflection.

Figures 6 and 7 show a consistent physical behavior. As the embedment ratio H/a increases, the stiffness of the medium also increases, and the static displacement

decreases (a_0=0). The dynamic behavior, on the other hand, shows an increasing oscillating behavior for larger values of the embedment parameter H/a.

4.3 Influence of the stiffness of the plate

Figures 8 to 10 show how the normalized central deflection w*(0), differential deflection w^*_d and bending moment $M^*_r(0)$ acting on a massless plate are affected by the stiffness of the plate, represented by the relative stiffness K_r (Eq. 90). Frequencies from the static case (a_0=0) up to a_0=4 are used. Two cases of embedment are shown: the plate at the interface between a half-space and a layer of thickness h_1/a=0.5 or two layers of thickness h_i=a. In all cases, the layers and the half-space are of the same homogeneous isotropic material and the loads are uniformly distributed.

Regardless of the frequency of excitation and depth of embedment, the amplitude of central and differential deflection decrease as the plate gets stiffer, while the amplitude of the bending moment increases accordingly. As expected, the differential displacement w^*_d goes to zero as the plate gets stiffer, and regardless of the frequency of excitation, its amplitude decreases for deeper embedments, since deeper embedments correspond to stiffer surrounding media. Notice that the static cases in all figures (a_0=0) correspond to those from Rajapakse (1988) (Fig. 4).

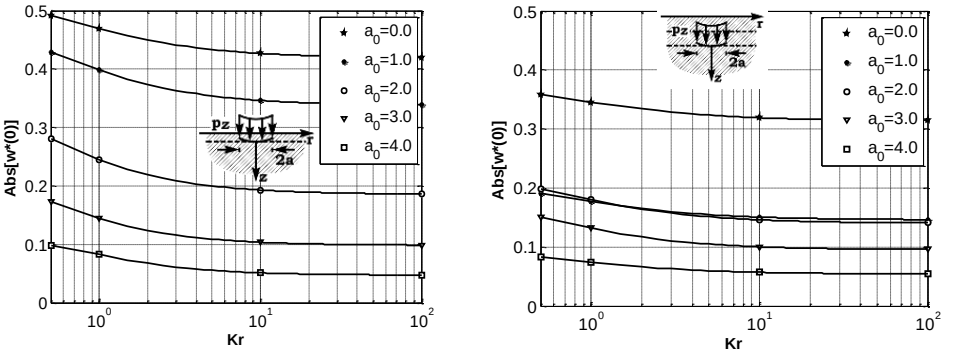

Figure 8: Influence of the stiffness of the plate on the central deflection of the plate under uniformly distributed loads, for embedments between a half-space and (a) a layer with thickness h_1/a=0.5 and (b) two layers of thickness h_i=a.

When looking at the behavior of the bending moment (Fig. 10), for example, it can be seen that the frequency of excitation that results in the smallest bending moment of a flexible plate (K_r=0.5) is not the same frequency that results in the

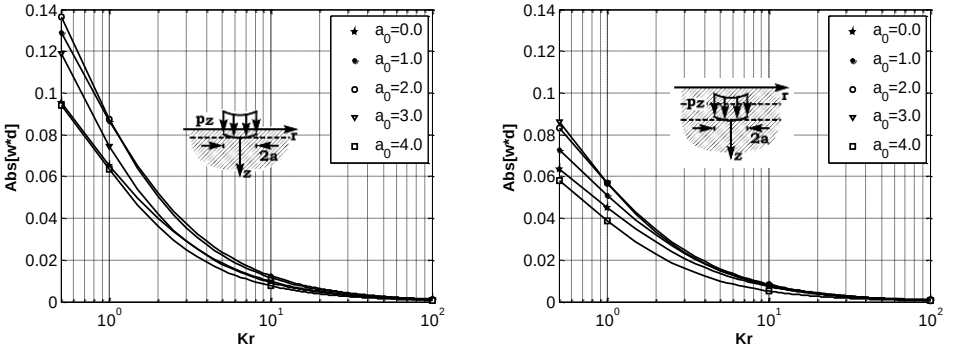

(a) (b)

Figure 9: Influence of the stiffness of the plate on the differential deflection of the plate under uniformly distributed loads, for embedments between a half-space and (a) a layer with thickness $h_1/a=0.5$ and (b) two layers of thickness $h_i=a$.

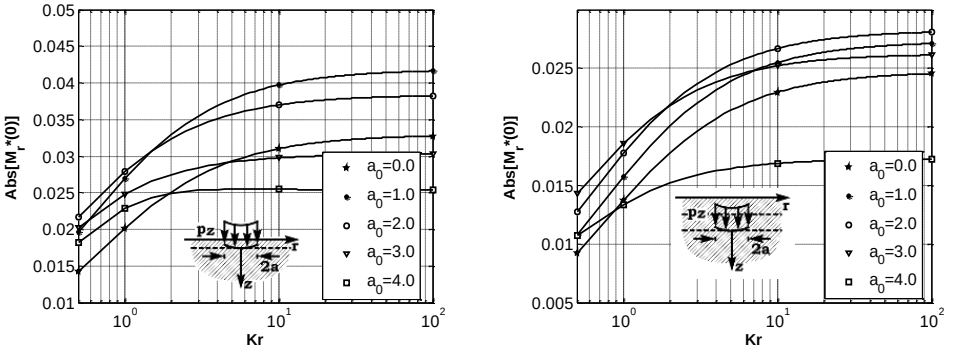

(a) (b)

Figure 10: Influence of the stiffness of the plate on the bending moment of the plate under uniformly distributed loads for embedments between a half-space and (a) a layer with thickness $h_1/a=0.5$ and (b) two layers of thickness $h_i=a$.

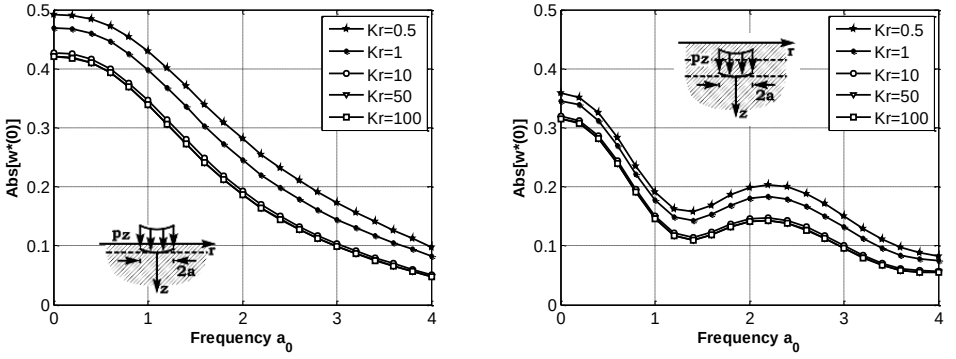

Figure 11: Influence of the stiffness of the plate on the central deflection of the plate under uniformly distributed loads for embedments between a half-space and (a) a layer with thickness $h_1/a=0.5$ and (b) two layers of thickness $h_i=a$.

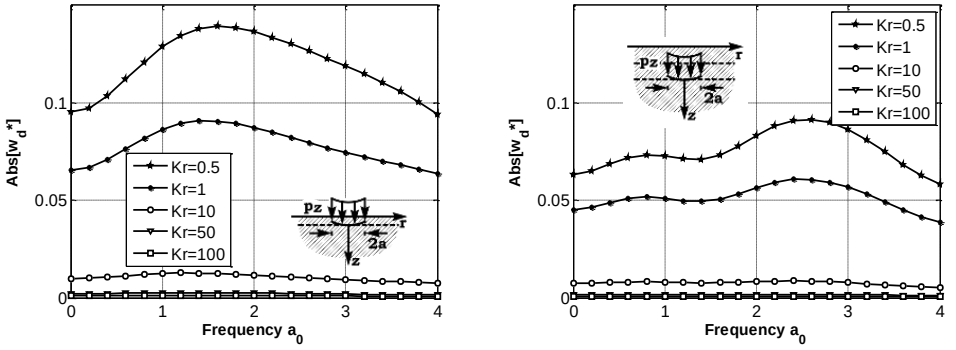

Figure 12: Influence of the stiffness of the plate on the differential deflection of the plate under uniformly distributed loads for embedments between a half-space and (a) a layer with thickness $h_1/a=0.5$ and (b) two layers of thickness $h_i=a$.

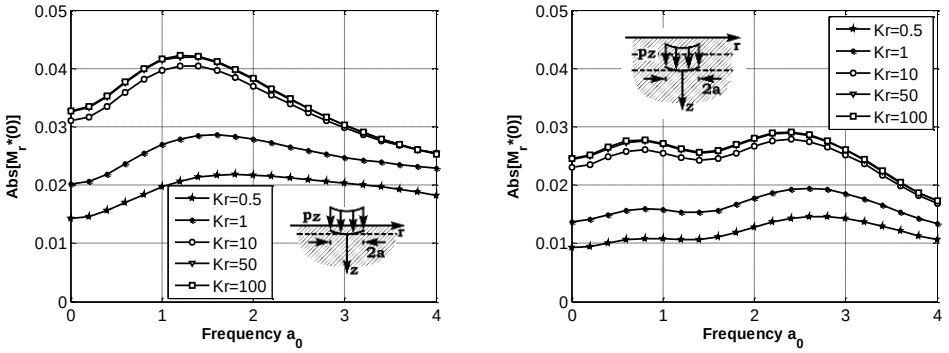

Figure 13: Influence of the stiffness of the plate on the bending moment of the plate under uniformly distributed loads for embedments between a half-space and (a) a layer with thickness $h_1/a=0.5$ and (b) two layers of thickness $h_i=a$.

smallest bending moment of a stiffer plate ($K_r >> 1$), regardless of the depth of embedment. It was seen in Figs. 6 and 7 that the deflection and moment acting on the plate are not monotonic curves and that their shape is strongly affected by the depth of embedment, but these new results show that the stiffness of the plate plays a relevant role in the amplitude of those curves. Figures 11 to 13 show this influence. The normalized central deflection $w^*(0)$, differential deflection w^*_d and bending moment $M^*_r(0)$ acting on the plate are shown for different relative stiffness K_r and depths of embedment.

4.4 Influence of the damping factor

In the present work, a model of hysteretic damping is introduced in the formulation according to the elastic-viscoelastic correspondence principle [Christensen, (2010)]:

$$c_{ij} = c^*_{ij}(1 + i\eta) \tag{93}$$

In Eq. (93), c^*_{ij} are the real elastic constants c_{11}, c_{12}, c_{13}, c_{33} and c_{44} that define the transversely isotropic material and c_{ij} are their complex counterparts that are used in the computer code. The hysteretic damping model considers that the damping factor η is a constant [Gaul, (1999)].

The representative embedment condition of the plate between a half-space and a layer of thickness $h_1/a=0.5$ is considered. Both the half-space and the layer are made of the same homogeneous isotropic material. Their damping coefficient is

varied between η=0.01 and η=0.2. Figure 14 shows the normalized central deflection w*(0) of a relatively flexible (K_r=0.5) and of a relatively stiff massless plate (K_r=100) under uniformly distributed loads.

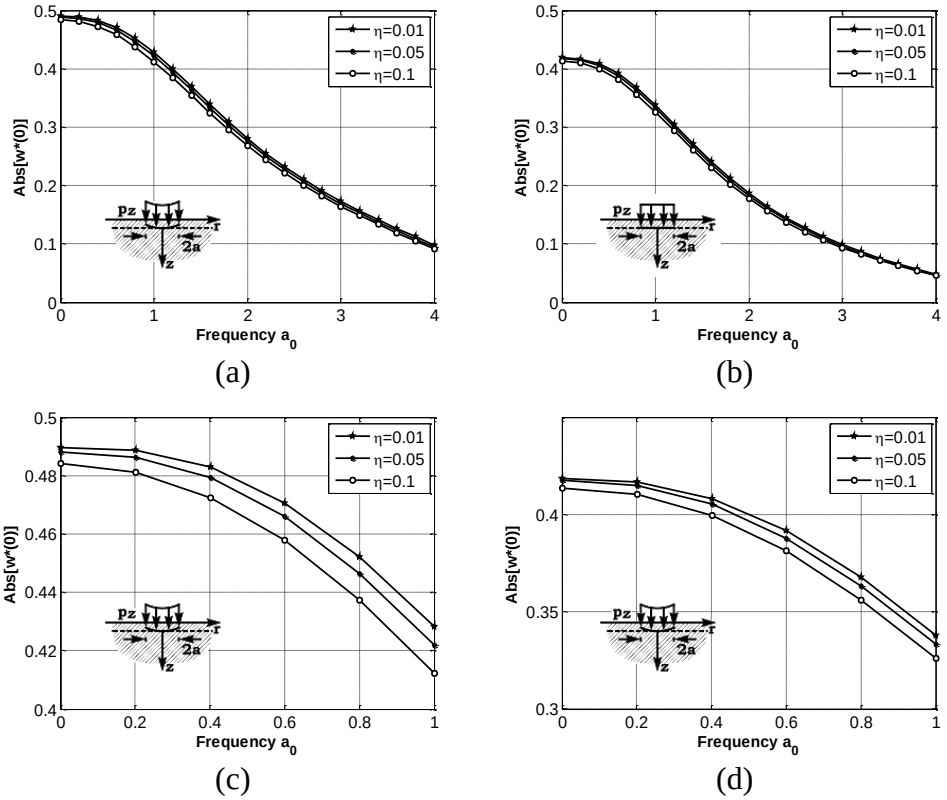

Figure 14: Influence of damping coefficient on the normalized central deflection w*(0) acting on a (a) relatively flexible plate (K_r=0.5) and (b) relatively stiff plate (K_r=100) under uniformly distributed loads. Figures (c) and (d) display the same results on a reduced frequency range ($0<a_0<1$).

The results obtained for the parameters chosen in this particular case (Fig. 14) show that higher damping coefficients stiffen the surrounding domain and cause an overall decrease in the displacement amplitude compared to the ones with smaller damping coefficients. This amplitude decay is supported by Gaul (1999). These results indicate that the strategy adopted in this work to represent the material attenuation in the transversely isotropic materials produces physically consistent results.

All results from sections 4.2 to 4.4 considered embedment of a massless plate

within an isotropic half-space so that the influence of loading configuration, frequency of excitation, depth of embedment, stiffness of the plate and damping coefficient of the surrounding medium could be separated from that of the composition of the layered system or the anisotropy of each layer.

4.5 Inertial response

The present formulation enables the study of cases of foundations possessing mass. The inclusion of mass is done by considering the kinetic energy of the plate according to Eq. (70). In this section, a representative case of a relatively flexible plate (Kr=0.5) of outer radius a, thickness h/a=0.1, Young's modulus E_p and Poisson's ratio ν_p is considered. The plate rests on the surface of a homogeneous half-space and its surface is under uniformly distributed unit loads.

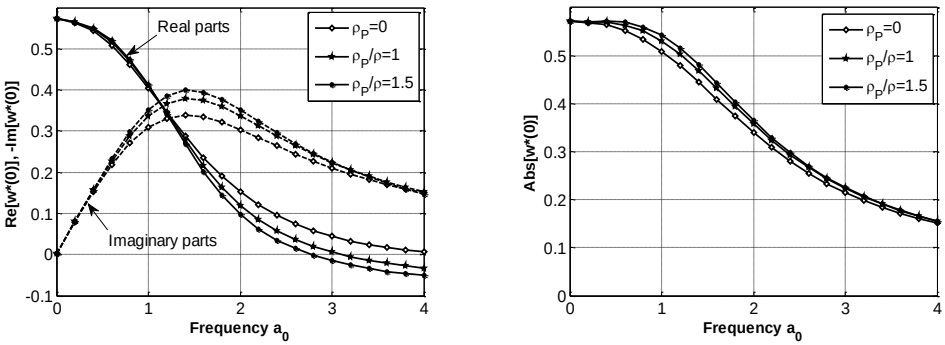

Figure 15: Central displacement of a flexible plate with different mass densities.

The results from Fig. 15 show how the central displacement of the plate is affected as the mass density of the plate ρ_P varies respective to that of the underlying half-space, ρ (Eqs. 1-3). For these particular cases, there is an increase in the amplitude of the displacement of the plate as the relative mass density increases.

4.6 Influence of layered construction

In this section, the bending of an elastic plate embedded in non-homogeneous layered media is investigated. Three different layered systems are considered (Fig. 16 and Tables 1 and 2). In all cases, the plate is embedded between two layers of thickness h_i=a (i=1,2) and a half-space. In all cases, the layers and the half-space are transversely isotropic materials with Poisson ratio ν=0.25 and damping coefficient η=0.01, while their other properties are obtained by varying an anisotropy index

$n=c_{33}/c_{11}$. The material of the layers and their thicknesses in each case are shown in Table 1. The material properties of the materials m_1, m_2 and m_3 are shown in Table 2. In Table 2, E_Z is the Young's modulus in the vertical direction, and ν_Z the Poisson ratio that relates deformations between the horizontal and vertical directions.

Table 1: Multilayered media configurations used in this section.

Layer	**Case A**	**Case B**	**Case C**
1	Material m_1; $h_1/a=0.5$	Material m_3; $h_1/a=0.5$	Material m_3; $h_1/a=0.3$
2	Material m_1; $h_2/a=0.5$	Material m_2; $h_2/a=0.5$	Material m_2; $h_2/a=0.7$
half-space	Material m_1; $h_3=\infty$	Material m_1; $h_3=\infty$	Material m_1; $h_3=\infty$

Table 2: Transversely isotropic materials used in this section ($c'_{ij}=c_{ij}/c_{44}$).

Material	**n**	$\mathbf{c'}_{11}$	$\mathbf{c'}_{12}$	$\mathbf{c'}_{13}$	$\mathbf{c'}_{33}$	**E'**	$\mathbf{E'}_Z$	ν	ν_Z
m_1	1.0	3.0000	1.0000	1.0000	3.0000	2.5	2.5000	0.25	0.2500
m_2	1.5	2.8284	0.8284	0.8284	4.2426	2.5	3.8673	0.25	0.2265
m_3	2.0	2.7749	0.7749	0.7749	5.5497	2.5	5.2114	0.25	0.2183

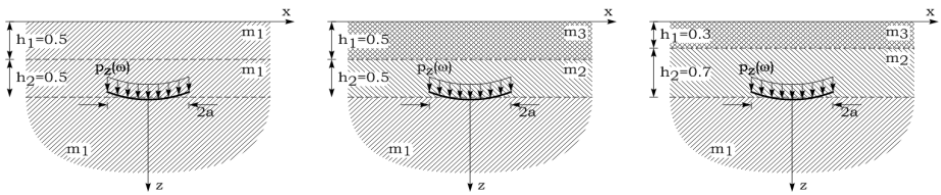

Figure 16: Illustration of different layered system configurations with an embedded plate subjected to uniformly distributed vertical loads.

Figures 17 to 19 show respectively the normalized deflection profile w*(r) of the plate, the normalized circumferential bending moment M_r*(r) and the normalized shear force Q*(r) acting on it, for the frequencies $a_0=0$ and $a_0=4$. All cases consider a uniformly distributed vertical load. In these results, the material properties E_s and ν_s considered in the relative stiffness K_r (Eq. 91) are those of the underlying half-space (material m_1 from Table 2).

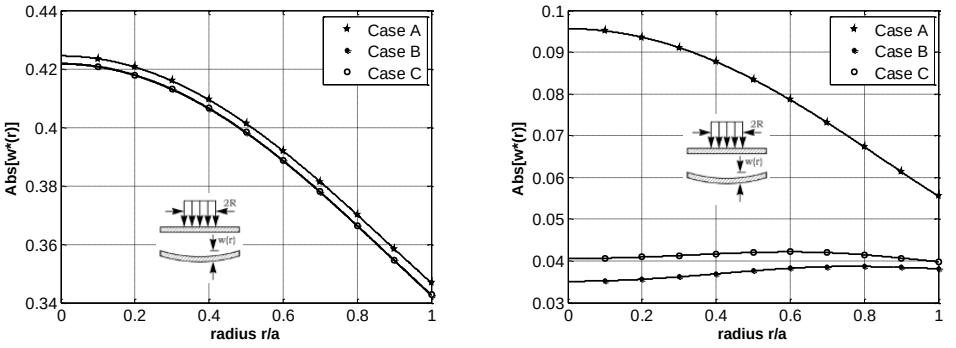

Figure 17: Normalized deflection profile w*(r) of a relatively flexible plate (K_r=0.5) under uniformly distributed loads, for different layered systems, for the frequencies (a) a_0=0 and (b) a_0=4.

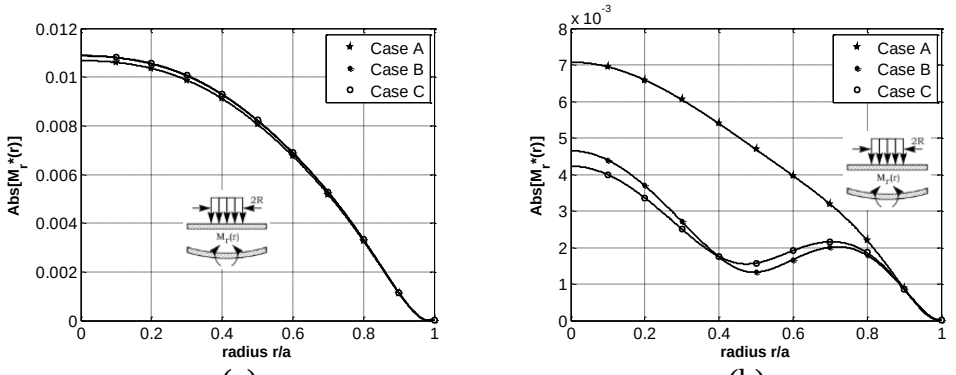

Figure 18: Normalized bending moment M_r*(r) acting on a relatively flexible plate (K_r=0.5) under uniformly distributed loads, for different layered systems, for the frequencies (a) a_0=0 and (b) a_0=4.

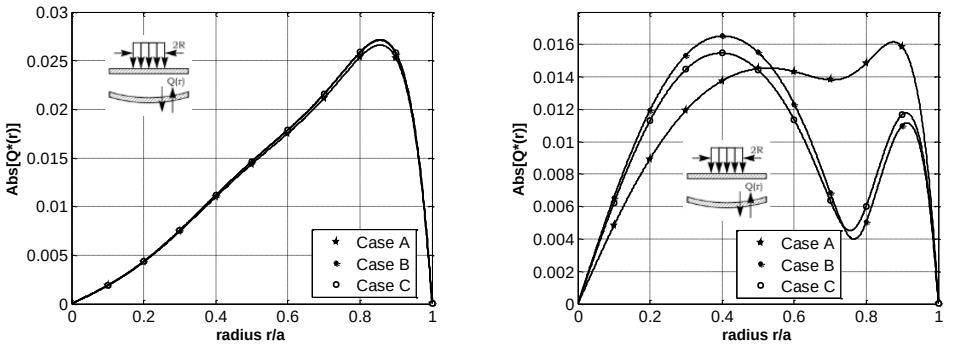

Figure 19: Normalized shear force Q*(r) acting on a relatively flexible plate (K_r=0.5) under uniformly distributed loads, for different layered systems, for the frequencies (a) a_0=0 and (b) a_0=4.

Notice that in all cases the moment M_r*(r) and the shear force Q*(r) satisfy the boundary conditions of free edge established in Eqs. 56 and 57. Moreover, the deflections of the plates shown in Fig. 17 are different than zero at the plate edge (w(r/a=1)≠0), which physically agrees with the boundary conditions of free edge.

Figure 17b enables an interesting physical interpretation of the problem. It is straightforward to observe, from that figure, that the most flexible surrounding medium (Case A) results in the largest displacement amplitudes. In cases B and C, the two layers on top of the plate are stiffer than those in Case A (Fig. 16). It can be seen that the displacement amplitude in both cases is smaller for these cases than for Case A, as expected (Fig 17b). Moreover, from Case B to Case C, the only difference is that the relative thickness of the layers changes toward the most flexible medium (layer 2). That is, the layered system in Case C is less stiff than in Case B. Consequently, Case C results in a larger displacement amplitude of the plate than Case B (Fig. 17b). This behavior is physically consistent and it holds for all results in this section, even though it is more clearly seen in Fig. 17b.

The overall conclusion from observing Figs. 17 to 19 is that the change in material composition has a more significant influence on the deflection of the plate than a change in the relative thickness of the layers, for the present embedment configurations. The variation between each Case, however, has little significance when compared to how much the magnitude of these quantities varies across the plate.

5 Concluding remarks

In the present paper, it is shown that the problem of an embedded flexible plate can be solved accurately by applying variational techniques, in which the solution of a constrained Lagrangian functional involving strain and kinetic energy of the plate and of its surrounding medium results in the deflection profile of the plate. The present implementation has been validated against existing results for homogeneous media in the literature. It has been observed that the amplitude of deflection of a plate decreases with increasing frequency of excitation, depth of embedment and plate stiffness. However, the combination of stiffness and frequency that results in the largest deflection amplitude is not obvious a priori. The general observation is that plates with higher flexibility under concentrated static loads at shallow embedments in low-damped media have the largest bending moment, shear force and deflection amplitudes. On the other hand, the smallest deflection, bending moment and shear force are observed for deeply embedded stiffer plates under uniformly distributed loads at higher frequency. The radius at which the maximum bending moment and shear force occur depends on the depth of embedment. As for the effects of non-homogeneous layered media on plate vibration, it was found that the bending moment, shear force and deflection are significantly more sensitive to parameters such as the loading area, depth of embedment, stiffness of plate, frequency of excitation and dissipation characteristics compared to the layered configuration or anisotropy of the surrounding medium.

Acknowledgement: The research leading to this article has been funded by the São Paulo Research Foundation (Fapesp) through grants 2012/17948-4, 2013/23085-1 and 2013/08293-7 (CEPID). The support of Capes, CNPq and Faepex/Unicamp is also gratefully acknowledged.

References

Abramowitz, M.; Stegun, I. A. (1965): *Handbook of Mathematical Functions with Formulas, Graphs, and Mathematical Tables*, New York: Dover.

Akbarov, S. D. (2013): On the Axisymmetric Time-Harmonic Lamb's Problem for a System Comprising a Half-Space and a Covering Layer with Finite initial Strains. *CMES – Computer Modeling in Engineering & Sciences*, vol. 95, no. 3, pp. 173-205.

Akbarov, S. D.; Hazar, E.; Eroz, M. (2013): Forced Vibration of the Pre-Stressed and Imperfectly Bonded Bi-Layered Plate Strip Resting on a Rigid Foundation. *CMC – Computers, Materials and Continua*, vol. 36, no. 1, pp. 23-48.

Barros, P. L. A. (1997): *Elastodinâmica de meios transversalmente isotrópicos:*

Funções de Green e o Método dos Elementos de Contorno na análise da interação solo-estrutura (Elastodynamics of Transversely Isotropic Media: Green's Functions and Boundary Element Method Analysis of the Soil-Structure Interaction). Ph.D. Thesis, University of Campinas, Campinas, Brazil.

Christensen, R. M. (2010): *Theory of Viscoelasticity*. New York, Dover Publications.

Crampin, S.; Chesnokov, E. M.; Hipkin, R. G. (1984): Seismic anisotropy— the state of the art. *Geophys. J., R. Astr. Soc*, vol. 76, no. 1, pp. 1-16.

Fung, Y. C. (1965): *Foundations of Solid Mechanics*, Prentice-Hall, Englewood Cliffs.

Fung, Y. C.; Tong, P. (2001): *Classical and Computational Solid Mechanics*, World Scientific Publishing Company.

Gaul, L. (1999): The Influence of Damping on Waves and Vibrations. *Mechanical Systems and Signal Processing*, vol. 13, no. 1, pp. 1-30.

Gucunski, N.; Peek, R. (1993): Vertical Vibrations of Circular Flexible Foundations on Layered Media, *Soil Dynamics and Earthquake Engineering*, vol. 12, pp. 183-192.

Kausel, E.; Peek, R. (1982): Dynamic loads in the interior of a layered stratum: an explicit solution, *Bull. Seism. Soc. Am.*, vol. 72, pp. 1459-1481.

Labaki, J. (2012): *Vibration of Flexible and Rigid Plates on Transversely Isotropic Layered Media.* Ph.D. Thesis, University of Campins, Campinas, Brazil.

Labaki, J.; Mesquita, E.; Rajapakse, R. K. N. D. (2013): Coupled Horizontal and Rocking Vibrations of a Rigid Circular Plate on a Transversely Isotropic Bi-Material Interface. *Engineering Analysis with Boundary Elements*, vol. 37, no. 11, pp. 1367–1377.

Marques de Barros, R. (2001): *Funções de Green e de Influência para meios visco-elásticos transversalmente isotrópicos no domínio da freqüência* (Green's functions and influence functions for viscoelastic, transversely isotropic media, in the frequency domain). Ph.D. Thesis, University of Campinas, Campinas, Brazil.

Mesquita, E.; Romanini, E. (1992): Green's function approach versus direct boundary element scheme to model the dynamic interaction of foundations resting on a viscoelastic layer over a bedrock. *Proc. IABEM (International Conference on Boundary Element Methods)*, 3-6 november, Seville, Spain, vol. 2, pp. 107-121.

Muki, R. (1960): Asymmetric problems of the theory of elasticity for a semi-infinite solid and a thick plate. I.N. Sneddon, R. Hill (Eds.), *Progress in Solid Mechanics*, vol. 1 North Holland, Amsterdam, pp. 399–439.

Pak, R. Y. S; Gobert, A. T. (1991): Forced Vertical Vibration of Rigid Discs with

Arbitrary Embedment. *J. Eng. Mech*, vol. 117, issue. 11, pp. 2527.

Payton, R. G. (1983): *Elastic Wave Propagation in Transversely Isotropic Media*. The Hague: Martinus Nijho.

Piessens, R.; Doncker-Kapenga, E. D.; Überhuber, C. W. (1983): *QUADPACK: a subroutine package for automatic integration*. Springer.

Rajapakse, R. K. N. D. (1988): The Interaction Between a Circular Elastic Plate and a Transversely Isotropic Elastic Half-Space. *International Journal for Numerical and Analytical Methods in Geomechanics*, vol. 12, pp. 419-436.

Rajapakse, R. K. N. D. (1989): Dynamic Response of Elastic Plates on Viscoelastic Half Space. *Journal of Engineering Mechanics*, vol. 115, no. 9, pp. 1867-1881.

Rajapakse, R. K. N. D; Wang, Y. (1993): Green's Functions for Transversely Isotropic Elastic Half Space. *Journal of Engineering Mechanics*, vol. 119, no. 9, pp. 1724-1746.

Romanini, E. (1995): *Síntese de funções de influência e Green para o tratamento da interação dinâmica solo-estrutura através de equações integrais de contorno*. Ph.D. Thesis, University of Campinas, Campinas, Brazil.

Seale, S. H.; Kausel, E. (1989): Point loads in cross-anisotropic layered half-spaces, *J. Engrg. Mech. ASCE*, vol. 115, pp. 509-524.

Selvadurai, A. P. S. (1979a): *Elastic Analysis of Soil-Foundation Interaction*, Elsevier, Amsterdam.

Selvadurai, A. P. S. (1979b): The interaction between a uniformly loaded circular plate and an isotropic elastic halfspace: A variational approach. *J. Struct. Mech.*, vol. 7, pp. 231-246.

Selvadurai, A. P. S. (1979c): An energy estimate of the flexural behaviour of a circular foundation embedded in an isotropic elastic medium. *International Journal of Numeric and Analytic Methods in Geomechanics*, vol. 3, pp. 285-292.

Selvadurai, A. P. S. (1980): The eccentric loading of a rigid circular foundation embedded in an isotropic elastic medium. *International Journal for Numerical and Analytical Methods in Geomechanics*, vol. 4, Issue. 2, pp. 121-129.

Sommerfeld, A. (1949): *Partial Differential Equations*, Academic Press, New York.

Timoshenko, S.; Woinowsky-Krieger, S. (1964): *Theory of Plates and Shells*, McGraw-Hill Classic Textbook Series.

Wan, F. Y. M. (2003): Stress boundary conditions for plate bending. *International Journal of Solids and Structures*, vol. 40, pp. 4107–4123.

Wang, Y. (1992): *Fundamental Solutions for Multi-Layered Transversely Isotropic*

Elastic Media and Boundary Element Applications. Ph.D. Thesis, University of Manitoba, Winnipeg, Canada.

Washizu, K. (1982): *Variational Methods in Elasticity and Plasticity*. 2^{nd} Ed, Pergamon Press, New York.

Wass, G. (1972): *Linear two-dimensional analysis of soil dynamics problems in semi-infinite layered media*. Ph.D thesis, University of California, Berkeley, California.

Wass, G. (1980): *Dynamics Belastete Fundamente auf Geschichtetemn Baugrund*, VDI Berichte, vol. 381, pp. 185-180 (in German).

Zaman, M. M. and Faruque, M. O. (1991): Mixed-Variational Approach for Restrained Plate-Half-Space Interaction. *J. Eng. Mech.*, vol. 117, pp. 1755-1770.

Zienkiewicz, O. C.; Kelly, D. W.; Bettess P. (1977): The Sommerfeld (Radiation) Condition on Infinite Domains and its Modelling in Numerical Procedures. *Computing Methods in Applied Sciences and Engineering*, I. Lecture Notes in Mathematics, vol. 704, pp 169-203.